THz Antenna-Coupled Microbolometer with 0.1-μm-wide Titanium Thermistor

International Journal of ChemTech Research
CODEN (USA): IJCRGG ISSN: 0974-4290
Vol.7, No.2, pp 1019-1026, 2014-2015

ICONN 2015 [4th - 6th Feb 2015]
International Conference on Nanoscience and Nanotechnology-2015
SRM University, Chennai, India

THz Antenna-Coupled Microbolometer with 0.1-μm-wide Titanium Thermistor

Ajay Tiwari[1], Hiroaki Satoh[1], Makoto Aoki[2], Masanori Takeda[2], Norihisa Hiromoto[2], and Hiroshi Inokawa[1]*

[1]Research Institute of Electronics, Shizuoka University, 3-5-1 Johoku, Naka-ku, Hamamatsu, 432-8011 Japan
[2]Graduate School of Engineering, Shizuoka University, 3-5-1 Johoku, Naka-ku, Hamamatsu, 432-8561 Japan

Abstract : Antenna-coupled microbolometers to detect terahertz wave were fabricated and their characteristics were evaluated at room temperature. The microbolometer consists of an integrated heater-thermistor and half-wave dipole antenna designed for 1 THz. The width of the Ti thermistor is made as narrow as 0.1 μm by electron beam lithography, and meander shape with longer effective length of thermistor is adopted to realize higher electrical resistance and to improve responsivity. The electrical responsivity for meander shape was 255 V/W, which was more than four times higher than that for the straight one. The electro-thermal circuit simulation was carried for better understanding of the observed results. Optical characterization of the bolometer with half-wave dipole antenna in the frequency range from 0.955 to 1.065 THz suggested that the Ti microbolometer was a promising device for detecting the electromagnetic waves in 1-THz frequency region.
Keywords: Far infrared (FIR), Terahertz (THz), Microbolometer, Electron beam lithography, Electro-thermal simulation.

Introduction

Detectors for far infrared (FIR) to terahertz (THz) waves are broadly classified into photon detectors and thermal detectors, both of them have generated a great deal of research interested over the last two decades[1-4]. Photon detectors are fast, more sensitive, and commercialized for military and space science applications but require cooling systems to reduce the dark current. On the other hand thermal detectors, represented by a microbolometer, have ability to work at room temperature. Moreover, uncooled FIR-THz detectors are low-cost, portability and more reliable, and have found many applications in areas such as surveillance, firefighting, night vision, military, etc[1]. However, uncooled bolometers have disadvantages, such as low detectivity due to thermal noise, response time, self-heating under constant bias[5], and susceptibility of the sensor material to the fabrication process[6]. Performance of such a microbolometer is mainly determined by (i) temperature coefficient of resistance (TCR) of the thermistor (ii) thermal isolation in the integrated structure of the heater and thermistor[7-9].

Microbolometer detectors measure the temperature change caused by absorbing electromagnetic waves as thermal energy. The size of the detector should be λ/n_e, where λ is the wavelength of electromagnetic radiation (i.e. 300 μm for 1 THz) and n_e is the effective refractive index. The effective refractive index is defined by $n_e = \sqrt{(1+\varepsilon')/2}$, where ε' is relative dielectric constant of the substrate[10,11]. The size of the detector would be 119 μm for Si substrate ε' = 11.699 and it is difficult to fabricate such a large size of absorption/thermistor film suspended above the air gap and to reduce the thermal capacitance and conductance.

Our group has recently proposed a novel structure for the THz microbolometer by adopting an antenna-coupled type[10,11]. The Au dipole antenna is made on the insulation layer of SiO_2 formed on a high-resistivity Si substrate. The heater of a resistor is placed at the center of the dipole antenna and the thermistor together with an insulation layer between them is stacked. The electric lines are connected to the thermistor to flow bolometer current and the take the signal out from the thermistor. Only the bolometer cell comprising of the heater, the insulation layer and the thermistor is suspended above the air gap holed in the substrate.

In order to evaluate the possibility antenna-coupled microbolometer detector, the 1-THz half-wave dipole antenna has the resonant antenna length of 52 μm on Si substrate and an integrated heater-thermistor, nominal length of the integrated heater-thermistor has to be reduced to about 10 μm (which is sufficiently shorter than the dipole-antenna length) in order to place in at the center of antenna, is fabricated, and its operation is analyzed.

We have verified scaling trend for integrated thermistor and heater before analyzing the properties of antenna-coupled microbolometer. The length dependences of the electrical responsivity and the cutoff frequency (f_c) of integrated thermistor and heater reveal that the former gets degraded and the latter improved as the length is reduced if the width and thickness of the heater-thermistor are kept the same[12,13]. To predict the responsivity and response speed, scaling trend is explicitly described in Table 1. The factor δ is used to represent the physical dimensions of heater and thermistor, and the change in parameters such as voltage, current, electrical and thermal resistances, and thermal capacitance is considered under constant-voltage condition. The overall effect of these parameters is reflected in the responsivity and the cutoff frequency. The cutoff frequency improve by length down scaling, but the responsivity is reduced by the same length reduction factor. To verify the scaling trend experimentally, the integrated thermistor and heater with different lengths were fabricated. The length dependence of electrical responsivity (R_v) and cutoff frequency (f_c) of integrated thermistor and heater is shown in Fig. 1. As it is obvious from the figure as predicted by the scaling trend, responsivity decreases with decreasing length. At 11 μm, the expected responsivity is ~110 V/W. But this length we have to choose as mentioned above, the nominal length ~ 10 μm (for integrated thermistor and heater) may be utilized for our antenna coupled devices.

Table 1. Scaling trend for microbolometer under constant-voltage condition

Parameters	Scaling factor	Remarks
Heater and / thermistor length	δ	
Heater and thermistor width, thickness	1, 1	
Voltage (V), Current (I), Input Power (P_{in})	1, δ^{-1}, δ^{-1}	
Electrical and thermal resistance (R_e and R_t)	δ	
Thermal Capacitance (C_t)	δ	
Temperature rise (ΔT)	1	$\propto P_{in} \times R_t$
Output Voltage (V_{out})	1	$\propto I \times R_e \times \Delta T$
Responsivity	δ	$\propto V_{out}/P_{in}$)
Cutoff frequency	δ^{-2}	$\propto 1/(R_t \times C_t)$

This degradation can be alleviated by more complex layout pattern of the thermistor, such as a meander shape, with longer effective length. As the result, electrical responsivity enhances, than that of the straight one. We have fabricated both straight and meander shape thermistors and compared their responsivities which will be discussed later.

In this paper, we describe a structure of a microbolometer coupled with a half-wave antenna on a Si substrate and observed electrical responsivity and cutoff frequency and compared it with the simulated results. The half-wave antenna characteristics are also verified from angle dependence of optical THz measurement.

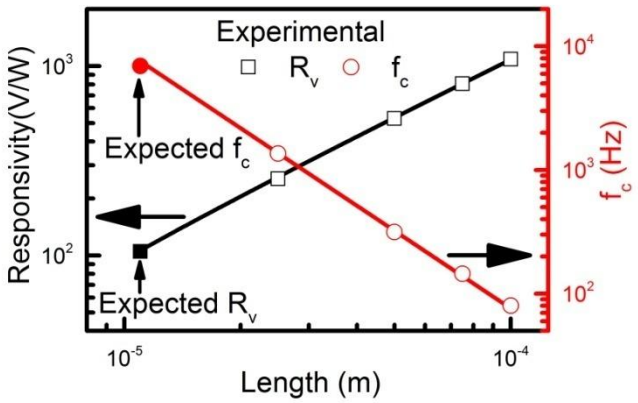

Fig. 1. Length dependence of responsivity (R_v) and cutoff frequency (f_c). Open square and circular symbols represent the R_v and f_c respectively while the closed square and circular symbols show the expected R_v and f_c respectively. Thickness and width of thermistor are 46 and 0.1 µm, respectively, and those of heater are 96 and 1.24 µm, respectively.

Microbolometer's structure

The microbolometer consists of gold (Au) antenna, titanium (Ti) heater, silicon dioxide (SiO_2) interlayer and Ti thermistor on thermally oxidized silicon (Si) substrate. The schematic diagram and scanning electron microscopic (SEM) pattern of the fabricated antenna-coupled microbolometer is illustrated in Fig. 2(a) and 2(b) respectively. The schematic diagram is used to give more insight of the integrated heater and thermistor part of the fabricated antenna-coupled microbolometer.

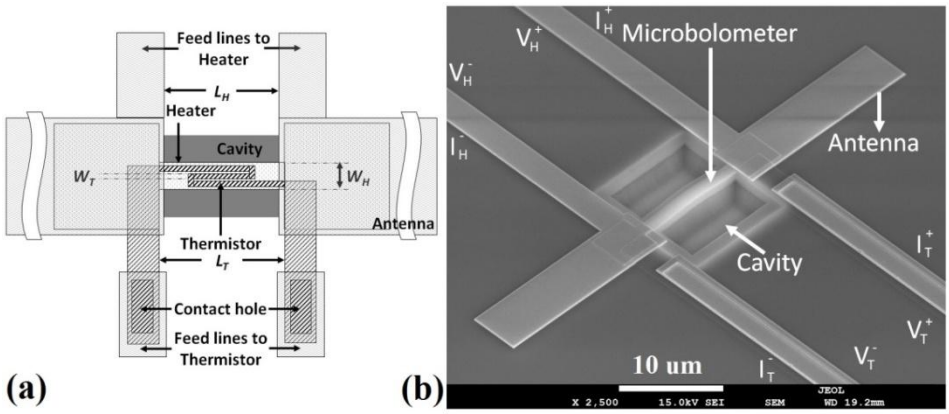

Fig.2.Antenna-coupled Tim icrobolometer. (a) Schematic diagram of the integrated thermistor/ interlayer/heater are at the center of the half-wave dipole antenna, (b) SEM image of microbolometer fabricated by electron beam lithography. Here I_T^- , I_T^+ and V_T^- , V_T^+ are current and voltage terminals respectively for thermistor, whereas I_H^- , I_H^+ and V_H^- , V_H^+ are similar terminals for heater.

The structure of the THz antenna-coupled microbolometer is as follows: A Au-metal antenna split at its center to two parts is made on a SiO_2 insulation layer formed on a high-resistivity Si substrate. A heater of a resistor is placed at the center of the antenna and directly connected to the antenna, a thermistor is electrically separated but thermally combined to the heater, and both of them are suspended on a cavity dug on a Si substrate.

Fabrication process

The process steps of microbolometer are discussed elsewhere[14]. The fabrication steps are as follows. The thermistor on thermally oxidized (TO) Si substrate was formed by lift off of electron beam evaporated Ti thin film pattern by electron beam lithography and as illustrated in Fig. 3 (a). The interlayer SiO_2 was deposited by electron cyclotron resonance (ECR) sputtering. The contact hole in ECR sputtered SiO_2 was created by CHF_3 reactive-ion etching (RIE) as shown in Fig. 3 (b). After that, heater was fabricated by lift off of patterned

evaporated Ti thin film as shown in Fig. 3 (c). The Au Antenna and electrical pads were fabricated by lift off of the patterned Ti/Au thin film as it is obvious in Fig. 3 (d). The deep-cavity for thermal isolation was formed by CHF_3 RIE and SF_6 plasma etching as shown in Fig. 3 (e). The scanning electron microscopy (SEM) image of meander shape thermistor pattern is shown in Fig. 3 (f), since the optical microscopy pattern resolution is not sufficient for 100 nm width thermistor. The Ti is selected considering its low thermal conductivity. The thermistor and heater are electrically separated by SiO_2 interlayer for independent optimization. The width of the Ti thermistor is made as narrow as 0.1 μm to attain high responsivity.

The fabricated antenna-coupled Ti microbolometer is shown is Fig. 2(b). As it is obvious from the figure, the available length for integrated thermistor and heater is ~10 μm. The heater and thermistor length should be ~ 10 μm. However this length can also be utilized for complex patterns, like meander shape thermistor pattern which is shown in the schematic diagram.

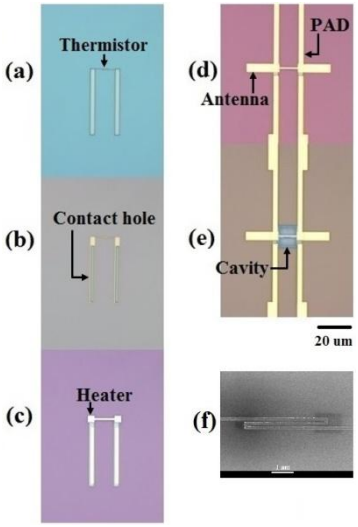

Fig. 3. The fabrication steps of Ti microbolometer (a) thermistor pattern, (b) contact hole in SiO_2 interlayer, (c) heater integrated on thermistor, (d) Au-antenna and electrical pads, (e) cavity for thermal isolation of integrated thermistor and heater and (f) SEM image of meander shape thermistor.

Electro-thermal simulation

To establish the correlation of the observed Ti microbolometer's responsivity, electro-thermal (E-T) circuit simulation was carried out using SPICE circuit simulator. The unit circuit representing heater/thermistor line with length ΔL, thermal resistance r_t, thermal capacitance c_t, electrical resistance r_e, and its temperature coefficient α is shown in Fig. 4(a), and the entire circuit is depicted in Fig. 4(b). Transient analysis was performed with sinusoidal input to V_{in} using SPICE circuit simulator, and the responsivity was calculated from the thermistor output with respect to heater input power for bias current 100 μA.

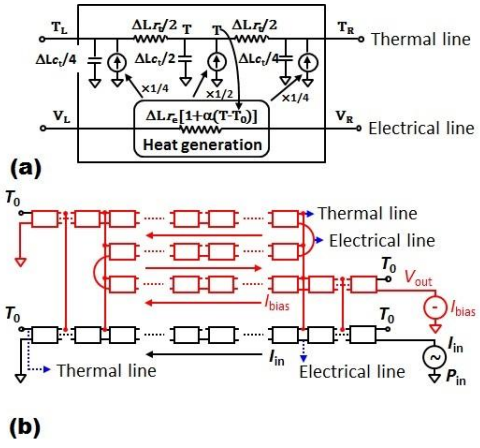

Fig. 4. Electro-thermal (E-T) circuit for simulation (a) unit circuit, and (b) entire circuit for integrated thermistor and heater for meander shape thermistor.

Results and discussion

After the device fabrication, the basic parameters were measured/calculated and listed in Table 2. Thickness of the heater/thermistor and antenna was measured by stylus profilometer, and width and lengths were designed values. Resistance and TCR were obtained by DC IV measurement at 240-300 K, and the values for 300 K are listed. Form the table it is clear that resistivity and TCR has width dependence. The detailed analysis of width dependence is out of the scope for the present report.

Table 2. Device parameters and their properties

Parameters	Heater (Ti)	Thermistor (Ti)	Antenna (Ti/Au)
Thickness (nm)	96	46	20/200
Width (μm)	1.24	0.1	5.2
Length (μm)	11	19.72	52
Resistivity (Ω.m)	$^{*}1.97 \times 10^{-6}$	$^{*}2.50 \times 10^{-6}$	$^{\$}4.18 \times 10^{-8}$
Temp. coef. (K^{-1})	1.25×10^{-3}	4.14×10^{-4}	
$SiO2^{TO}$ thickness (nm)	208		
$SiO_2{}^{ECR}$ thickness (nm)	87		
Cavity depth (μm)	3.2		

*Bulk Ti resistivity = 4.78×10^{-7} Ω.m

$^{\$}$Bulk Au resistivity = 2.27×10^{-8} Ω.m

Thermal resistance of the heater and thermistor line was evaluated based on the phenomenon that the electrical resistance of the thermistor increases with increasing DC current. The increase of the normalized resistance as function of square of the current is shown in Fig. 5 for both (a) independent thermistor and (b) integrated thermistor. The normalized resistance linearly increases with the square of the current. For an isolated wire, the resistance change was observed and discussed analytically by Zhang *et al*[15]. The experimental data was fitted by using Zhang *et al.* approach and determined the average temperature rise, which is also shown in Fig. 5 for both (a) and (b) type thermistor. Input fitting parameters for the simulation are thermal resistance per unit length of the heater (r_t), thermal capacitance(c_t), electrical resistance per unit length (r_e) and temperature coefficient of resistance (α), which are 6.73×10^{11} K/(Wm), 1.34×10^{-6} J/Km, 1.50×10^{7} Ω/m , and 1.253×10^{-3}, respectively for heater. Similarly for thermistor they are 3.76×10^{13} K/(Wm), 9.99×10^{-9} J/Km, 6.68×10^{8} Ω/m , and 4.14×10^{-4}, respectively. The experimentally obtained thermal conductances are 1.20 W/(mK) for SiO_2 and 5.78 1.20 W/(mK) for Ti, however the reported values are 1.32 W/(mK) for SiO_2 and 21.9 W/(mK) for Ti[16,17]. The extracted value of thermal conductance of Ti is approximately ~4 times lower than the reported values in the literature. The resistivity is ~ 4 times higher than the bulk value of Ti (as shown in Table 2). From Wiedemann-Franz law, it is expected that lower value of thermal conductance for heater Ti will show higher value of resistivity, that is what we have observed. Using the above parameters the E-T circuit simulation was carried out to estimate the responsivity and cutoff frequency for the microlometer.

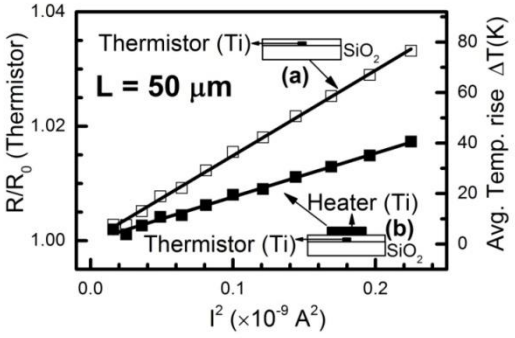

Fig. 5. Dependence of $\Delta R/R_0$ on I^2 for independent thermistor (a) and integrated thermistor/heater (b) for 50 μm length.

The responsivity of the fabricated microbolometers is measured by applying AC electrical power up to 2 μW at 100 Hz. Thermistor output was detected by lock-in amplifier under the bias current of 100 μA. Thermistor output voltage with respect to the heater input power is shown in Fig. 6 (a) for straight and meander shape thermistors. The observed responsivity values are 57 and 255 V/W for straight and meander shapes, respectively.

For straight shape thermistor, the simulated responsivity is very high as compared to experimental one. The expected experimental responsivity (as shown in Fig. 1) is ~110 V/W but we did not get the expected experimental value. It may have happened due to partial isolation of the integrated thermistor/heater from the Si substrate. The present etching depth for isolation in Si is 3.2 μm (see Table 2), which seems to be not sufficient for perfect isolation.

For meander shape thermistor, the experimentally observed responsivity is lower than the simulated one. One of the reasons may be the use of the fixed value of TCR in simulation. We have used TCR value at 300 K, however in reality the average temperature rise is ~50 K (*e.g.* as shown in Fig. 5), and actual TCR is lower. The other possibility may be due to the bias current of the thermistor. Since extra heat produced during microbolometer operation, which was not taken in to account while estimating the values of thermal resistance for both thermistor and heater from the individual I-V measurements. During the I-V measurement either thermistor or heater was used at a time but during microbolometer operation, both thermistor with 100 μA current and heater with 2 μW power produce heat, which has been ignored in the extraction of input parameters for E-T simulation.

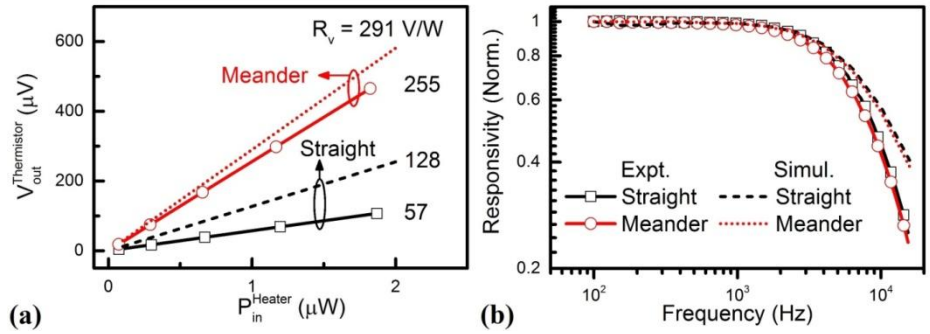

Fig. 6. The experimental and simulated results of Ti microbolometer (a) Thermistor output versus heater input power for straight and meander shape thermistor at 100 Hz, and (b) frequency response of Ti microbolometer for straight and meander shape thermistor at 2 μW input power. The symbol shows the experimental result, while dashed and dotted lines show simulated result.

In order to determine the cut-off frequency of our fabricated detector, the frequency response measurement are performed for both type of thermistors. To compare them, normalized frequency response are plotted for both thermistors as shown in Fig. 6(b). The simulated frequency responses are also shown to compare with the experimental one. This also validates of extracted thermal capacitances for our device dimension. The frequency response of both straight and meander shape matches very well with the simulated one as illustrated in Fig. 6(a) and 6(b). The slight different between experimentally observed frequency response to the simulated one may be due to frequency response characteristics of the V/I converter which we have used during measurement to when we apply input power to the heater.

The THz responsivity is measured by using electromagnetic radiation emitted from a 1 THz source with three-stage Schottky-barrier amplitude-multiplier chains multiplying by 72 times the microwave from a synthesizer[18]. The THz response distributing on the full frequency range from 0.955 THz to 1.065 THz of the 1THz-source and the response cutoff frequency of 7 kHz, which are consistent with the results of the electromagnetic, thermodynamic and E-T circuit simulations of the antenna-coupled detector as discussed above in Fig. 6. The thermistor response of the THz antenna-coupled bolometer is dependent on the direction of the polarization of the THz radiation, which demonstrate the detention of the radiation by the dipole antenna and illustrated in Fig. 7.

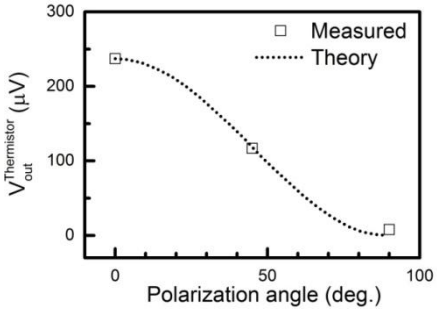

Fig. 7. Thermistor signal of the room temperature THz antenna-coupled microbolometer responding to the 1 THz radiation as a function of the polarization angle of the radiation. The polarization angles of 0 and 90 degrees are on the E-plane and the H-plane, respectively. [Ref. 18]

The measured highest responsivity is 90 V/W at 1.012 THz and the corresponding noise-equivalent power (NEP) is 4.6×10^{-10} W/Hz$^{1/2}$ suggesting that Ti microbolometer is a promising device for detecting the electromagnetic waves around 1 THz frequency region.

Conclusion

An antenna-coupled Ti microbolometer was designed and fabricated using electron beam lithography. The responsivity of the straight and meander shape of the Ti thermistor with 0.1 μm width are compared. The use of meander shape enhances the responsivity compared to straight one. The experimental results were also assessed by E-T circuit simulation and compared. The lower value of experimental responsivity compared to simulated result may be due to the fixed value of TCR used for simulation or incomplete thermal isolation in the fabricated bolometer. The polarization angle dependence of the optical measurement validates the characteristics of half-wave dipole antenna.

Acknowledgement

This study is partially supported by Industry-Academia Collaborative R & D from Japan Science and Technology Agency, JST.

References

1. Kruse P. W., Uncooled IR focal plane array, Proc. SPIE, 1995, 2552; 556-563.
2. Kruse P. W., Uncooled IR focal plane array, Opto-electronics review, 1999, 7(4); 253-258.
3. Rogalski A., Infrared detectors: status and trends, Progress in Quantum Electronics, 2003, 27; 59-210.
4. Rogalski A. and Sizov F.,Terahertz detectors and focal plane arrays, Opt. Elec. Rev. 2011, 19 (3); 346-404.
5. Ramakrishna M.V.S., Karunasiri G., Neuzil P., Sridhar U. and Zeng W. J., Highly sensitive infrared temperature sensor using self-heating compensated microbolometers, Sensor. Actuator. A, 2000, 79; 122-127.
6. Chen S., Ma H., Xiang S. and Yi X., Fabrication and performance of microbolometer arrays based on nanostructured vanadium oxide thin films, Smart Mater. Struct., 2007, 16; 696-700.
7. Hiromoto N., "Terahertz detectors and sensing for the ground use," 9th Takayanagi Kenjiro Memorial Symposium & 4th International Symposium on Nanovision Science (Hamamatsu, Japan, Oct. 30, 2007).
8. Zerov V. Y., Malyarov V. G., and Khrebtov I. A., Antenna-coupled microbolometers, J. Opt. Technol., 2011, 78; 308-316.
9. Tanaka A., Matsumoto S., Tsukamoto N., Itoh S., Chiba K., Endoh T., Nakazato A., Okuyama K., Kumazawa Y., Hijikawa M., Gotoh H., Tanaka T., and Teranishi N., Infrared focal plane array incorporating silicon IC process compatible bolometer, IEEE Trans. Electron Devices, 1996, 43;1844-1850.
10. Aoki M., Takeda M., and Hiromoto N. Electromagnetic simulation for THz antenna-coupled microbolometers operated at room temperature, Makara Seri Teknologi, 2013, 17 (1); 1-6.

11. Aoki M., Takeda M., and Hiromoto N. Electromagnetic and thermal simulation for room temperature THz antenna-coupled microbolometers, Inter-Academia 2012, 27-30 August, Budhapest, Hungry, 65-74.
12. Tiwari A., Satoh H., Aoki M., Takeda M., Hiromoto N. and Inokawa H., Scaling Study of Antenna-Coupled Microbolometer, 46th conference on Solid State Devices and Materials (SSDM), PS-7-14 (Tsukuba, Japan, Sept. 8-11, 2014).
13. Tiwari A., Satoh H., Aoki M., Takeda M., Hiromoto N. and Inokawa H., Length Dependence of Microbolometer Characteristics, 61st conference on Japan Society of Applied Physics (JSAP), 18p-E17-18 (Japan, March. 17-20, 2014).
14. Tiwari A., Satoh H., Aoki M., Takeda M., Hiromoto N. and Inokawa H., Analysis of Microbolometer Characteristics for Antenna-Coupled Terahertz Detectors, Aisan J. Chem., 2013, 25; S358-S360.
15. Zhang S., Yang Y., Sadeghipour S. M. and Asheghi M., Thermal Characterization of the 144 nm GMR Layer using Microfabricated Suspended Structures, Proceedings of ASME Summer Heat Transfer Conference, paper HT 2003-47270 (Las Vegas, Nevada, USA, July 21-23, 2003).
16. Kato R. and Hatta I., Thermal Conductivity and Interfacial Thermal Resistance: Measurements of Thermally Oxidized SiO_2 Films on a Silicon Wafer Using a Thermo-Reflectance Technique, Int J. Thermophys 2008, 29; 2062-2071.
17. http://en.wikipedia.org/wiki/Titanium
18. Hiromoto N., Tiwari A., Aoki M., Satoh H., Takeda M. and Inokawa H., Room-Temperature THz Antenna-Coupled Microbolometer with a Joule-Heating Resistor at the Center of a Half-Wave Antenna, 39th conference on Infrared, Millimeter Terahertz Waves (IRMMW-THz) R3/A-27.6 (Univ. Arizona, Tucson, AZ, USA, Sep. 14-19, 2014).

*****